



High-entropy alloy: challenges and prospects

Y.F. Ye, Q. Wang, J. Lu, C.T. Liu and Y. Yang*

Centre for Advanced Structural Materials, Department of Mechanical and Biomedical Engineering, City University of Hong Kong, Tat Chee Avenue, Kowloon Tong, Kowloon, Hong Kong

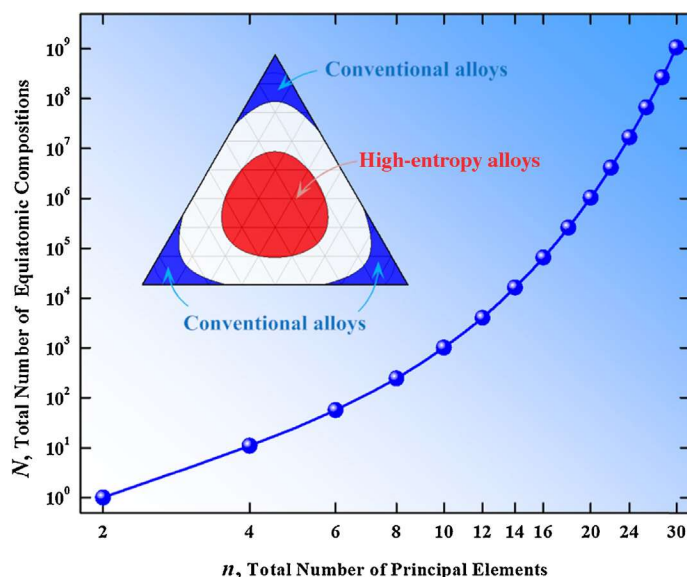
High-entropy alloys (HEAs) are presently of great research interest in materials science and engineering. Unlike conventional alloys, which contain one and rarely two base elements, HEAs comprise multiple principal elements, with the possible number of HEA compositions extending considerably more than conventional alloys. With the advent of HEAs, fundamental issues that challenge the proposed theories, models, and methods for conventional alloys also emerge. Here, we provide a critical review of the recent studies aiming to address the fundamental issues related to phase formation in HEAs. In addition, novel properties of HEAs are also discussed, such as their excellent specific strength, superior mechanical performance at high temperatures, exceptional ductility and fracture toughness at cryogenic temperatures, superparamagnetism, and superconductivity. Due to their considerable structural and functional potential as well as richness of design, HEAs are promising candidates for new applications, which warrants further studies.

Introduction

From ancient times, human civilization has striven to develop new materials [1], discovering new metals and inventing new alloys that have played a pivotal role for more than thousands of years. Since the Bronze Age, alloys have traditionally been developed according to a 'base element' paradigm. This strategy begins with one and rarely two principal elements, such as iron in steels or nickel in superalloys, and a minor alloying approach is used to obtain alloys with enhanced properties. In sharp contrast, a novel paradigm for alloy design was proposed about a decade ago [2,3], which involves merely the mixing of multiple elements in an equimolar or near-equimolar composition to form alloys, thus eschewing the 'base element' concept. These designed multicomponent alloys were termed as 'high-entropy alloys' (HEAs) by Yeh et al. [2], which suggests the high configurational entropy of the random mixing of elements in these alloys. Presently, HEAs are being increasingly studied [2,4–8]. Nevertheless, given the short history of research on HEA, the field is still in its infant stage in comparison to that of conventional alloys.

When designing alloys, researchers previously focused on the corners of a phase diagram to develop a conventional alloy, which occupy only a small portion of the design space, as illustrated by the inset of Fig. 1. However, with the advent of HEAs, the focus has been shifted to the central region. Conceptually, this is a radical departure from conventional theories [2,3,9], opening up new avenues of alloy design to be explored in depth. In principle, with the conventional 'base element' approach, only n types of alloys can be obtained using n different base elements. However, if any combination of p elements were to be selected from the total of n elements to form an equiatomic alloy ($p = 2, 3, \dots, n$), the total number, N , of possible alloys can be increased from n to $N = 2^n - n - 1$. When n is < 3 , the strategies do not differ considerably; however, with increasing n , this difference can grow because of the exponential dependence of N on n . As shown in Fig. 1, one can obtain $N \sim 10^6$ possible equiatomic alloys for $n = 20$; this number (N) can even reach up to about one billion for $n = 30$! In the literature [2], Yeh defined HEAs as alloys containing at least five elements. Even if this convention were followed, the total number of possible HEA compositions remains considerably high, even increasing tremendously as about 75% of the 118-element

*Corresponding author: Yang, Y. (yonyang@cityu.edu.hk)

**FIGURE 1**

The variation in the total number of equiatomic compositions with the total number of principal elements. The inset illustrates the difference between the design of conventional alloys and high-entropy alloys on a ternary plot.

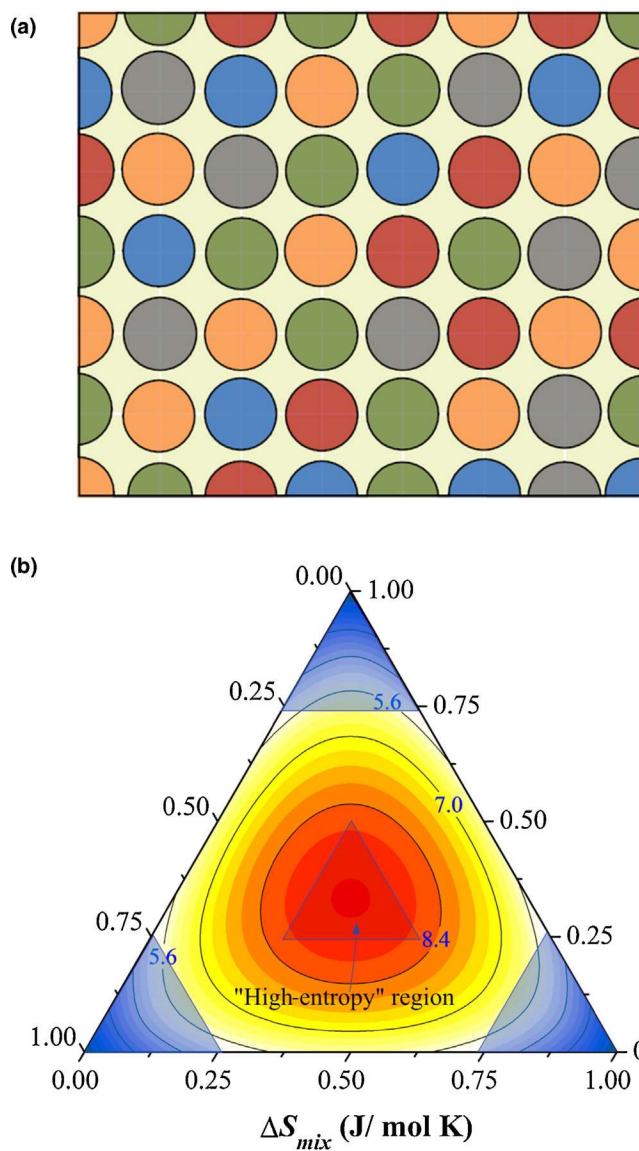
periodic table comprises metals. Conceptually, this poses a great challenge, both theoretically and experimentally, to materials scientists when studying HEAs with novel, valuable properties for real applications.

The concept of HEAs

One of the central themes of the ongoing research on HEAs is understanding the possible interplay between mixing entropy and phase selection in HEAs. In this respect, the following question emerges: what is the mixing entropy in an HEA? In previous studies [2,3], the term 'high-entropy alloy' was used because the alloy may have been modeled as an ideal solution, as illustrated in Fig. 2a. Therefore, the configurational entropy of mixing per mole could be expressed as $\Delta S_{mix} = -R \sum_{i=1}^n c_i \ln c_i$, where R is the gas constant, c_i the molar fraction of the i th element, and n the total number of the constituent elements [2,10]. As an example, Fig. 2b shows the contour map of ΔS_{mix} for a model ternary alloy. As observed in this figure, the closer the alloy composition to the central region the larger the ΔS_{mix} value, which reaches a maximum of 9.15 J/mol K at the very center. A total energy gain of $T_m \Delta S_{mix} \sim 20 \text{ kJ/mol}$ is observed for a typical alloy with a melting point of $T_m \sim 2000 \text{ K}$. According to Richard's rule [10], in most metallic alloys, this energy gain is sufficient for the entropic stabilization of a random solid solution phase against intermetallic compounds. Consequently, the mixing entropy, ΔS_{mix} , for an equiatomic HEA is given by [2]

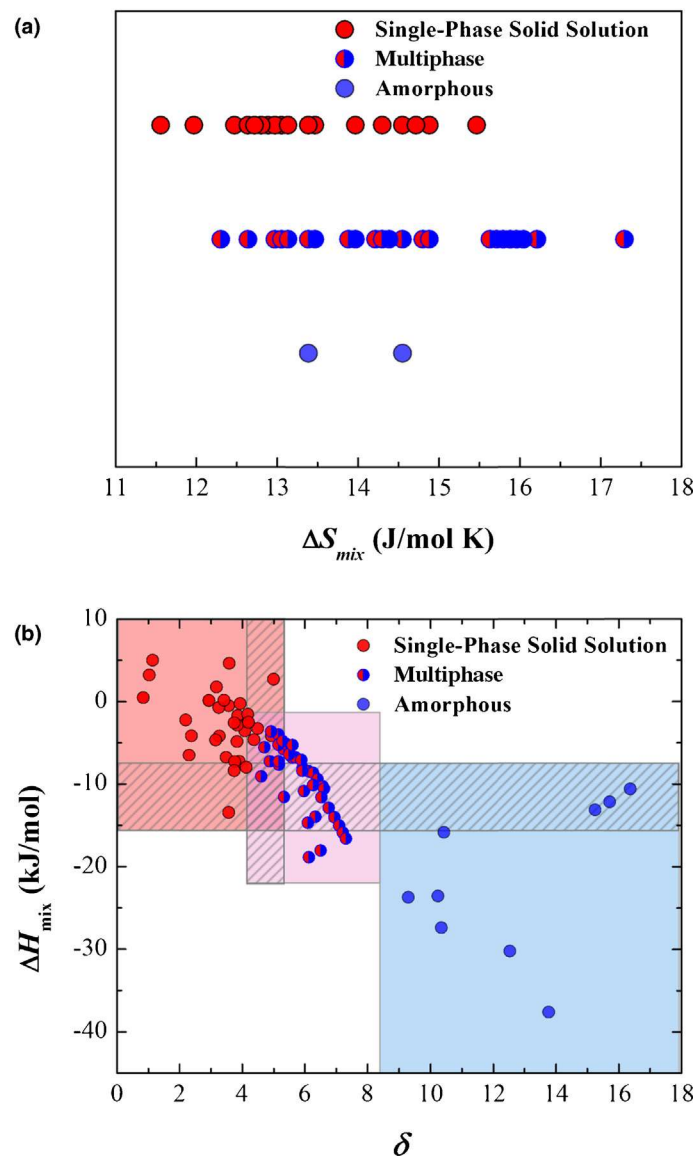
$$\Delta S_{mix} = R \ln n \quad (1)$$

In line with the 'high-entropy' effect, the random solid solution could be stabilized against the intermetallic compounds when numerous elements were mixed in an equimolar fraction. As ΔS_{mix} scales with $\ln n$, a larger ΔS_{mix} could be obtained for alloys with a greater number of constituent elements, thus increasing the possibility of forming solid solutions, according to Eqn 1 [2].

**FIGURE 2**

(a) The illustrated concept of random mixing of elements, as represented by the circles in different colors, in a multicomponent alloy. With equal atom size and loose atomic packing implicitly assumed, the configuration entropy of mixing of the alloy is equivalent to that of an ideal gas, thus being maximized via the equiatomic composition design. (b) The contour plot of ΔS_{mix} (J/mol K) on a schematic ternary alloy system. The blue corner regions indicate the conventional alloys based on one or two principal elements, whereas the red center region indicates the 'high-entropy' region.

Although the calculation of the mixing entropy of an HEA was straightforward when Eqn 1 was used, not only solid solutions but also a large amount of other phases, such as intermetallic compounds and even metallic glasses [3,11–16], were detected at room temperature in the cast HEAs. As shown in Fig. 3a, such a phase diversity indicates that ΔS_{mix} cannot be solely used as a parameter in the design of HEAs. Thus, Eqn 1 might have overestimated the real mixing entropy of a multicomponent alloy. Furthermore, as noted by different research groups [5,17–19], Eqn 1 may apply only to high temperatures, finding no direct use in calculating the mixing entropy at low temperatures. Alternatively, Zhang et al. [9] proposed the use of two additional parameters for the design of HEAs,

**FIGURE 3**

The plot of (a) ΔS_{mix} and (b) ΔH_{mix} versus δ for as-cast HEAs with different phases. Note that several amorphous compositions share the same ΔS_{mix} on (a).

namely, the atomic size difference δ and the mixing enthalpy ΔH_{mix} [9]:

$$\delta\% = 100\% \sqrt{\sum_{i=1}^n c_i \left(1 - \frac{r_i}{\sum_{j=1}^n c_j r_j}\right)^2} \quad (2)$$

where c_i and r_i denote the atomic fraction and atomic radius of the i th element, respectively. Zhang et al. also proposed the following equation [9]:

$$\Delta H_{\text{mix}} = \sum_{i=1, i \neq j}^n \Omega_{ij} c_i c_j = \sum_{i=1, i \neq j}^n 4\Delta H_{ij}^{\text{mix}} c_i c_j \quad (3)$$

where $\Delta H_{ij}^{\text{mix}}$ is the enthalpy of mixing of the binary liquid between the i th and j th elements at an equiatomic composition. Figure 3b displays the plot of ΔH_{mix} versus δ for about 90 different types of as-cast HEAs (Table 1 for details). As observed in Fig. 3b, HEAs generally tend to form single-phase solid solutions in the

case of low mixing enthalpy and atomic size difference. In general, the formation of a single-phase solid solution corresponds to the region $-15 \text{ kJ/mol} < \Delta H_{\text{mix}} < 5 \text{ kJ/mol}$ and $0 < \delta < 5$, which is in line with the summarized results of Zhang et al. [5]. Different phases then appear with the increase in ΔH_{mix} and δ . With the further increase in $\delta (> 8)$ and decrease in the negative ΔH_{mix} value ($< -15 \text{ kJ}$), upon casting, HEAs can even form metallic glass as a metastable structure, in line with the empirical rules of Inoue [20]. Evidently, the two-parameter (ΔH_{mix} vs. δ) approach offers better descriptors than the original one-parameter (ΔS_{mix}) approach when screening HEAs with different phases. However, the 'entropic' difference between HEAs and conventional alloys, if any, can be eliminated by exploiting ΔH_{mix} and δ .

The discrepancy between the theory (Eqn 1) and experiments (Fig. 3a) can be elucidated through the assumptions underlying Eqn 1. When deriving Eqn 1, it is implicitly assumed that all constituent elements should be of identical atomic size and loose arrangement [4,10,18,19], as observed in an ideal solution. However, this does not hold for real alloys, whose constituent elements can differ significantly in their atomic sizes, as illustrated in Fig. 4a, and show dense packing [13,18,19] at low temperatures. Therefore, in principle, their mixing entropy depends not only on their chemical composition but also their atomic size and packing density [4,5,18,19,21]. This is observed particularly in cases of the atomic packing density of an alloy increasing at low temperatures. According to Mansoori et al. [22], the total configurational entropy of mixing S_T per sphere for a hard sphere system with different-sized particles can be expressed as follows:

$$S_T(c_i, r_i, \xi) = S_C(c_i) + S_E(c_i, r_i, \xi) \quad (4)$$

where $S_C = -k_B \sum_{i=1}^n c_i \ln c_i$ is the configurational entropy of mixing for an ideal solution, which is equivalent to ΔS_{mix} in Eqn 1, and k_B is Boltzmann's constant. In Refs [4,18,22], S_E was defined as the excessive entropy of mixing, which is generally a function of the atomic composition c_i , the atom size r_i , and the overall packing density ξ . It is worth noting that the functional form of S_E is significantly involved, which is detailed in Ref [18], and is therefore omitted here for brevity.

When applying Eqn 4 to HEAs, it is given that the total mixing entropy of a multicomponent alloy is also a function of atomic size due to the presence of S_E . In general, S_E is negative in sign [18,22,23], and S_T is therefore less than S_C . As shown in Fig. 4b, the magnitude of S_E decreases with a decrease in the atomic packing density ξ and disappears when ξ becomes very small. Therefore, S_T approaches its maximum value, S_c , only in the case of negligibly small ξ . As the packing density ξ of an alloy generally decreases with increase in temperature, Fig. 4b indicates that S_c provides a good approximation of the mixing entropy of an alloy only for high temperatures, as expected previously. Nevertheless, at low temperatures or high packing densities, S_T could be considerably lower than S_c or ΔS_{mix} for a given alloy.

The dependence of S_T on atomic size has very important implications. First, an equiatomic composition might not effectively maximize the configurational entropy of mixing of an alloy. As exemplified by the ternary plot of the model Mn-Ni-Fe alloy (Fig. 4c), the chemical composition that maximizes the mixing entropy is located within the central region of the ternary plot, although it deviates from the equiatomic composition at low

TABLE 1

Calculated parameters δ , ΔH_{mix} , S_c , VEC, φ , and ε_{RMS} .

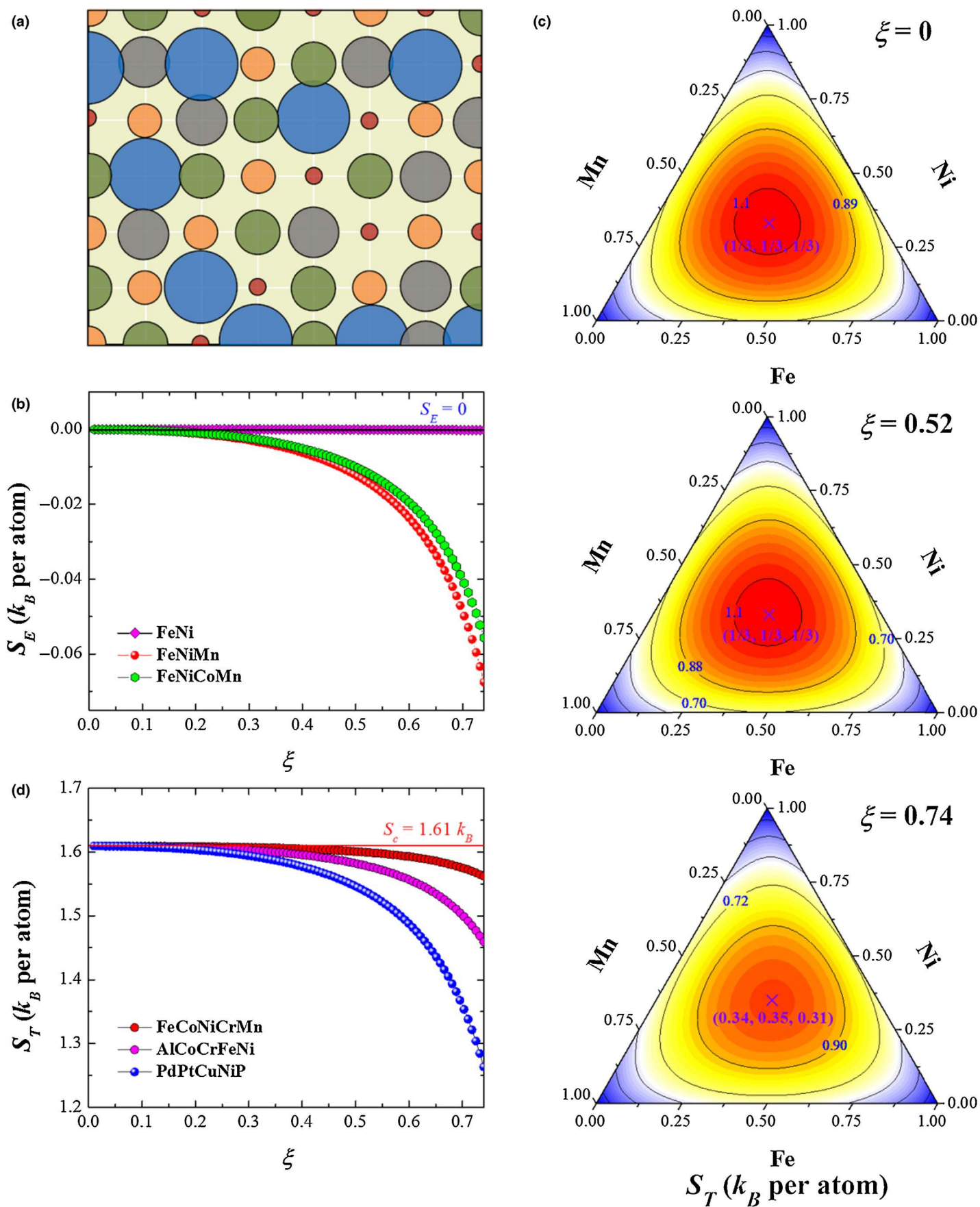
Alloy composition	δ	ΔH_{mix} (kJ/mol)	S_c (k_B per atom)	φ	ε_{RMS}	VEC	Phase detected
Al_{0.5}CoCrCuFeNiAl_{0.2}	4.93	-4.15	1.86	17.41	0.0487	8.12	FCC [76]
Al_{0.3}CoCrFeNi	3.76	-7.27	1.54	19.99	0.0370	7.88	FCC [77]
Al_{0.5}CrCuFeNi₂	4.20	-2.51	1.52	20.44	0.0414	8.45	FCC [78]
CoCrFeNi	0.30	-3.75	1.39	3583.31	0.0039	8.25	FCC [79]
CoFeMnNi	3.55	-4.00	1.39	24.51	0.0353	8.50	FCC [79]
CoCrMnNi	3.45	-5.50	1.39	23.99	0.0343	8.00	FCC [79]
CoCrFeNiPd	4.46	-7.04	1.61	15.95	0.0446	8.80	FCC [38]
CoCrCu_{0.5}FeNi	0.84	0.49	1.58	627.50	0.0083	8.56	FCC [80]
CuNiCoFeCrAl_{0.5}V_{0.2}	4.15	-2.50	1.86	26.49	0.0409	8.16	FCC [81]
CuNiFeCrMo	3.58	4.64	1.61	28.97	0.0356	8.20	FCC [48]
CuNiCoFe	1.14	5.00	1.39	223.55	0.0114	9.50	FCC [82]
CuNiCoFeMn	3.18	1.76	1.61	41.04	0.0316	9.00	FCC [36]
CuNi₂FeMn₂Cr	3.57	-0.49	1.55	33.58	0.0356	8.43	FCC [83]
CuNi₂FeCrAl_{0.2}	2.94	0.12	1.44	44.59	0.0289	8.77	FCC [84]
CuNi₂FeCrAl_{0.4}	3.86	-1.70	1.50	24.87	0.0381	8.56	FCC [84]
CuNi₂FeCrAl_{0.5}	4.20	-2.51	1.52	20.44	0.0414	8.45	FCC [84]
Cu_{0.75}NiCoFeCrAl_{0.25}	3.25	-0.71	1.72	42.39	0.0320	8.40	FCC [85]
Cu_{0.5}NiCoFeAl_{0.5}Cr	4.37	-4.60	1.75	20.16	0.0431	8.00	FCC [85]
Cu_{0.5}NiCoCrAl_{0.5}Fe₂	4.08	-3.53	1.68	23.06	0.0403	8.00	FCC [11]
Cu_{0.5}NiCoCrAl_{0.5}Fe₃	3.84	-2.84	1.57	24.99	0.0379	8.00	FCC [11]
Cu_{0.5}NiCoCrAl_{0.5}Fe_{3.5}	3.74	-2.58	1.52	25.76	0.0368	8.00	FCC [11]
FeCoNiCrCu	1.03	3.20	1.61	369.34	0.0103	8.80	FCC [35]
FeNi₂CrCuAl_{0.2}	2.94	0.12	1.44	44.59	0.0289	8.77	FCC [28]
FeCrMnNiCo	3.27	-4.16	1.61	34.71	0.0325	8.00	FCC [3]
FeCoNiCrCuAl_{0.3}	3.42	0.16	1.79	44.96	0.0337	8.47	FCC [35]
FeCoNiCrCuAl_{0.5}	4.17	-1.52	1.77	25.77	0.0411	8.27	FCC [35]
FeNi₂CrCuAl_{0.6}	4.49	-3.27	1.53	17.39	0.0443	8.36	FCC [28]
NiCoFeCrMo_{0.3}	2.38	-4.15	1.54	62.10	0.0235	8.09	FCC [86]
NiCoFeCrMo_{0.1}Al_{0.3}	3.90	-7.26	1.62	20.05	0.0385	7.84	FCC [86]
NiCoFeCrAl_{0.25}	3.48	-6.75	1.53	23.78	0.0342	7.94	FCC [77]
NiCoFeCrAl_{0.3}	3.76	-7.27	1.54	19.99	0.0370	7.88	FCC [86]
NiCoFeCrAl_{0.375}	4.12	-7.99	1.56	16.16	0.0406	7.80	FCC [77]
VcuFeCoNi	2.20	-2.24	1.61	84.95	0.0220	8.60	FCC [9]
TaNbHfZrTi	4.99	2.72	1.61	16.90	0.0499	4.40	BCC [58]
TaNbVTi	3.93	-0.25	1.39	26.07	0.0397	4.75	BCC [87]
TaNbVTiAl_{0.25}	3.83	-4.82	1.53	25.84	0.0387	4.65	BCC [87]
TaNbVTiAl_{0.5}	3.74	-8.40	1.58	24.28	0.0377	4.56	BCC [87]
TaNbVTiAl_{1.0}	3.57	-13.44	1.61	20.38	0.0360	4.40	BCC [87]
WnbMoTa	2.31	-6.50	1.39	60.87	0.0231	5.50	BCC [15]
WnbMoTaV	3.15	-4.64	1.61	41.18	0.0315	5.40	BCC [15]
Al₂₀Li₂₀Mg₁₀Sc₂₀Ti₃₀	5.16	-0.4	1.56	16.17	0.0515	2.8	HCP [50]
GdTbDyTmLu	5.07	0	1.61	18.76	0.0515	3	HCP [16]
HoDyYGdTb	0.81	0	1.61	701.52	0.0081	3	HCP [88]
YgdTbDyLu	1.37	0	1.61	245.87	0.0137	3	HCP [16]
AlCo₃CrCu_{0.5}FeNi	4.88	-7.25	1.62	12.52	0.0482	7.93	Multiphase [89]
Al_{0.8}CrCuFeMnNi	5.15	-3.97	1.79	15.73	0.0512	7.66	Multiphase [90]
AlCo₂CrCu_{0.5}FeNi	5.17	-7.67	1.71	11.83	0.0511	7.77	Multiphase [89]

TABLE 1 (Continued)

Alloy composition	δ	ΔH_{mix} (kJ/mol)	S_c (k_B per atom)	φ	ε_{RMS}	VEC	Phase detected
AlCrCuFeMnNi	5.39	-5.11	1.79	13.54	0.0536	7.50	Multiphase [90]
Al _{0.5} CoCrFeNi	4.60	-9.09	1.58	12.23	0.0454	7.67	Multiphase [77]
Al _{0.5} CoCrCuFeNiTi _{0.4}	5.49	-6.42	1.90	13.02	0.0543	7.98	Multiphase [76]
Al _{0.5} CrFeNiCoCuTi _{0.6}	5.92	-8.40	1.92	10.36	0.0586	7.85	Multiphase [76]
Al _{0.5} CrFeNiCoCuTi _{0.8}	6.26	-10.11	1.92	8.54	0.0621	7.73	Multiphase [76]
Al _{0.5} CoCrCuFeNiTi _{1.0}	6.53	-11.60	1.93	7.23	0.0649	7.62	Multiphase [76]
Al _{0.5} CoCrCuFeNiTi _{1.2}	6.76	-12.89	1.92	6.26	0.0671	7.51	Multiphase [76]
Al _{0.5} CoCrCuFeNiTi _{1.4}	6.94	-14.02	1.91	5.47	0.0690	7.41	Multiphase [76]
Al _{0.5} CoCrCuFeNiTi _{1.6}	7.09	-15.01	1.90	4.85	0.0706	7.31	Multiphase [76]
Al _{0.5} CoCrCuFeNiTi _{1.8}	7.21	-15.86	1.89	4.34	0.0719	7.22	Multiphase [76]
Al _{0.5} CoCrCuFeNiTi _{2.0}	7.31	-16.60	1.88	3.91	0.0729	7.13	Multiphase [76]
CoCrFeNiTi _{0.5}	5.33	-11.56	1.58	7.91	0.0525	7.78	Multiphase [91]
CoCrFeNiAlNb _{0.25}	6.10	-14.66	1.72	5.26	0.0605	7.10	Multiphase [9]
CoCrFeNiAlNb _{0.75}	6.50	-18.03	1.79	3.95	0.0648	6.91	Multiphase [9]
CoCrCuFeNiTi _{0.8}	5.70	-6.75	1.79	11.12	0.0563	8.14	Multiphase [70]
CoCrCuFeNiTi	6.12	-8.44	1.79	8.92	0.0605	8.00	Multiphase [70]
CuAlNiCoCrFeSi	6.13	-18.86	1.95	4.15	0.0610	7.29	Multiphase [33]
CuNi ₂ FeCrAl _{0.9}	5.15	-5.22	1.56	12.08	0.0509	8.08	Multiphase [84]
CuNi ₂ FeCrAl _{1.2}	5.60	-6.78	1.57	9.25	0.0556	7.83	Multiphase [84]
CuNi ₂ FeCrAl _{1.5}	5.93	-8.05	1.57	7.47	0.0589	7.62	Multiphase [84]
Cu _{0.5} Ti _{0.5} CrFeCoNiAl _{0.5}	5.97	-10.84	1.89	8.79	0.0591	7.64	Multiphase [92]
CuCoNiCrAlFeTiV	6.34	-13.94	2.08	7.73	0.0631	7.00	Multiphase [34]
FeNi ₂ CrCuAl	5.32	-5.78	1.56	10.94	0.0526	8.00	Multiphase [28]
FeNi ₂ CrCuAl _{1.2}	5.60	-6.78	1.57	9.25	0.0555	7.84	Multiphase [28]
FeCoNiCrCuAl _{0.8}	4.92	-3.61	1.79	17.15	0.0487	8.00	Multiphase [35]
FeCoNiCrCuAl	5.28	-4.78	1.79	14.12	0.0523	7.83	Multiphase [35]
FeCoNiCrCuAl _{1.5}	5.89	-7.05	1.78	9.90	0.0585	7.46	Multiphase [35]
FeCoNiCrCuAl _{2.0}	6.26	-8.65	1.75	7.62	0.0623	7.14	Multiphase [35]
FeCoNiCrCuAl _{2.3}	6.40	-9.38	1.73	6.70	0.0638	6.97	Multiphase [35]
FeCoNiCrCuAl _{2.8}	6.57	-10.28	1.68	5.53	0.0656	6.71	Multiphase [35]
FeCoNiCrCuAl _{3.0}	6.61	-10.56	1.67	5.17	0.0661	6.63	Multiphase [35]
FeCoNiCuAl	5.61	-5.28	1.61	10.44	0.0556	8.20	Multiphase [93]
MnCrFe _{1.5} Ni _{0.5} Al _{0.3}	4.70	-5.51	1.48	13.89	0.0470	7.19	Multiphase [94]
MnCrFe _{1.5} Ni _{0.5} Al _{0.5}	5.16	-7.26	1.52	10.62	0.0510	7.00	Multiphase [94]
ErTbDyNiAl	13.74	-37.60	1.61	-2.24	0.1429	4.40	Amorphous [95]
PdPtCuNiP	9.29	-23.68	1.61	-1.26	0.0952	9.20	Amorphous [25]
SrCaYbMgZn	15.25	-13.12	1.61	-0.017	0.1565	4.20	Amorphous [84]
SrCaYbMgZn _{0.5} Cu _{0.5}	16.37	-10.60	1.75	0.61	0.1699	4.10	Amorphous [95]
SrCaYbLi _{0.55} Mg _{0.45} Zn	15.71	-12.15	1.75	0.2	0.1612	4.09	Amorphous [95]
TiZrCuNiBe	12.53	-30.24	1.61	-0.9	0.1268	6.20	Amorphous [12]
ZrHfTiCuNi	10.34	-27.36	1.61	-0.27	0.1049	6.60	Amorphous [96]
ZrHfTiCuFe	10.43	-15.84	1.61	1.73	0.1059	6.20	Amorphous [96]
ZrHfTiCuCo	10.24	-23.52	1.61	0.42	0.1039	6.40	Amorphous [96]

temperatures. Takeuchi et al. [19] recently reported similar predictions. Second, alloys with the same number of constituting elements may not exhibit the same configuration entropy of mixing S_T . Figure 4d shows the total entropy of mixing, S_T , as a function of ξ calculated for FeCrMnNiCo, AlCoCrFeNi, and

PdPtCuNiP, respectively. Although all of these alloys have five constituent elements and share the same S_c value of $1.6 k_B$, in the as-cast state, FeCrMnNiCo displays a single-phased face-centered cubic (FCC) structure [3] and AlCoCrFeNi a mixed body-centered cubic (BCC) and FCC structure [24], whereas PdPtCuNiP becomes

**FIGURE 4**

(a) The illustrated concept of random mixing of elements, as represented by the circles in different colors and of varying sizes, in a multicomponent alloy. In this case, the configurational entropy of mixing of the alloy depends not only on the chemical composition but also on the atom size and packing. It is

an excellent bulk metallic glass former [25]. Evidently, the formulation of the total entropy of mixing, S_T , can identify HEAs that exhibit phase diversity unexplained by the formulation of S_c or ΔS_{mix} alone.

Phase selection in HEAs: the theoretical approach

The equilibrium thermodynamic method aims to determine the phase stability in an HEA by computing the Gibbs free energy of different phases that could possibly form in a certain HEA. A direct comparison identifies the phase that is more energetically favorable. This direct approach enables the prediction of the exact phases, although this requires data on all possible phases for that alloy; further, it is generally difficult to perform for multicomponent alloys using simulation methods based on physical potentials, such as classical molecular dynamics simulations [5,26]. Consideration of metastable phases, such as metallic glasses, introduces more challenges. Alternatively, empirical and semiempirical rules have also been proposed to understand phase stability and guide the design of HEAs [4,8,18,19,27,28]. Compared with the direct computational approach [5,14,26,29,30], discussed subsequently, these rules have been mainly established by comparing the theoretical models with the existing experimental data; therefore, they can be applied to both equilibrium and metastable phases.

Thermodynamic rules

According to Yeh and coworkers [2], HEAs are alloys comprising multiple principal elements whose configurational entropy of mixing dominates the thermodynamics of solidification, which thus favors the formation of a random solid solution against intermetallic compounds. Symbolically, the proposal by Yeh et al. [2] may be translated as follows:

$$TS_{sys} \gg \max\{|H_i|\} \quad (i = 1, 2, \dots, m) \quad (5)$$

where S_{sys} is the configurational entropy of mixing of the alloy system and H_i the formation enthalpy of the i th phase, assuming m possible phases in total. As a result, the HEAs that satisfy Eqn 5 are solidified into a single-phase structure because of the negligible effect of formation enthalpy as hypothesized previously. It should be noted that Eqn 5 was not strictly derived based on the existing rules of thermodynamics; however, it has been proven useful for one to claim the entropic dominance in a multicomponent alloy according to the results reported in the literature [2,3,14,19,21,31–34]. The phase selection rule for HEAs is discussed in detail subsequently.

In their early work, Yeh et al. [2] proposed a criterion of $\Delta S_{mix} \geq \ln(5)R = 1.6R$ for casting an HEA, which corresponds to the mixing of at least five elements in an equiatomic composition. Comparing this criterion with Eqn 5 and assuming $S_{sys} \sim \Delta S_{mix}$, the simple criterion of Yeh et al. appears to hold if the temperature T is much higher than the critical value $T_c = \max\{|H_i|\}/1.6R$. If $\max\{|H_i|\} \sim |\Delta H_{mix}|$ is assumed, as in Refs [5,13,21,27], T_c is estimated to be on the order of a few hundred Kelvins for typical HEAs, such as

FeCoNiCrCu [35], FeCoNiCrMn [3], and CuNiCoFeMn [36]. However, for HEAs with low $|\Delta H_{mix}|$, the estimated T_c could be as small as a few Kelvins. Alternatively, the entropic gain can be computed relative to the magnitude of the mixing enthalpy $|\Delta H_{mix}|$ by fixing T at T_m , the alloy's melting point, which can be approximated based on the rule of mixture [27]. Similarly, Zhang et al. [27,37] proposed using the following parameter Ω to guide the design of HEAs:

$$\Omega = \frac{T_m \Delta S_{mix}}{|\Delta H_{mix}|} \quad (6)$$

Comparing Eqn 6 with Eqn 5, one can infer that, by assuming $\max\{|H_i|\} \sim |\Delta H_{mix}|$ and $S_{sys} \sim \Delta S_{mix}$, the dimensionless parameter Ω measures the energy gain as the mixing entropy is relative to that of enthalpy. The corollary in this case is that the larger the Ω the higher the probability of forming a single-phase random solid solution in HEAs and vice versa. However, as noted in Fig. 5a, the Ω values computed for the HEAs with different phases significantly overlap. This behavior suggests that, similar to S_c (Fig. 3a), Ω cannot be used as the sole descriptor of phase selection in HEAs either; instead, it should be used in combination with other thermodynamic and topological parameters related to the constituent elements [37].

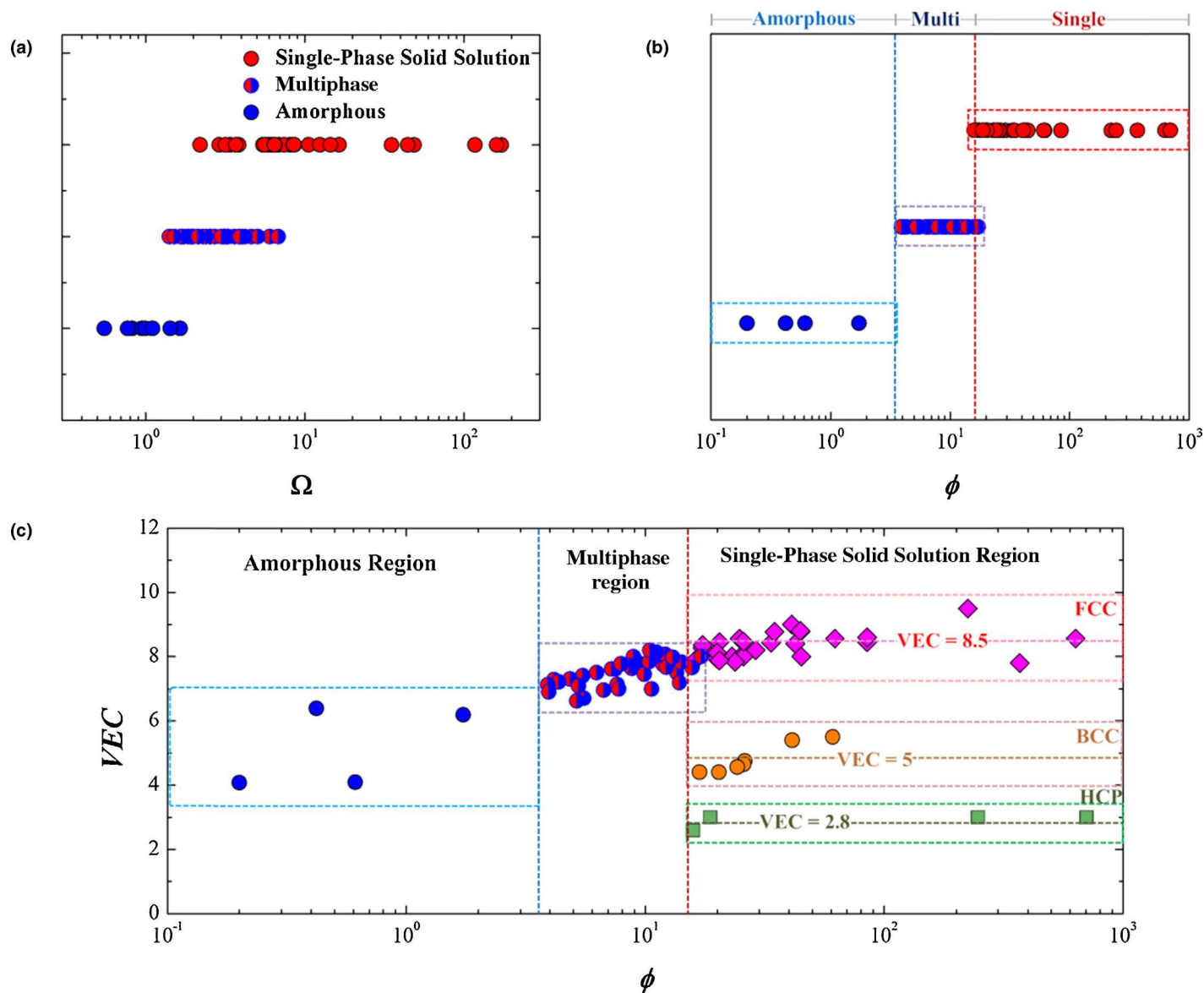
Taking account of the generality of S_T in formulating the configuration entropy of mixing of HEAs at both high and low packing densities [4,18]. Ye et al. assumed $S_{sys} \sim S_T = S_c - |S_E|$ (Eqn 4). Consequently, they proposed a new parameter ϕ by assuming $T = T_m$ and $\max\{|H_i|\} \sim |\Delta H_{mix}|$ to guide the design of HEAs [4]:

$$\phi = \frac{S_c - |\Delta H_{mix}|/T_m}{|S_E|} \quad (7)$$

In line with Eqn 5, it can be expected that the larger the ϕ the higher the probability of forming a single-phase solid solution in HEAs. As clearly observed in Fig. 5b, the HEAs show different groupings according to their corresponding ϕ values. HEAs with different phases are separated at a critical value of $\phi_c = 20$. Evidently, the HEAs display single-phase solid solutions when $\phi > \phi_c$ and multiphased and even amorphous structures when $\phi < \phi_c$. This behavior suggests that ϕ is a promising descriptor for ranking HEAs by their propensity to form single-phase solid solutions. Here, it is worth noting that the ϕ_c value is empirically determined by comparison with the experimental data on the X-ray diffraction (XRD) spectra of as-cast HEAs. Therefore, the ϕ_c value may change if these alloys are subsequently subjected to annealing. Apart from the empirical determination of ϕ_c , the ϕ criterion can be better improved by approximating $\max\{|H_i|\}$ as the average formation enthalpy $|H_f|$ of the HEAs based on the data provided by Tropparovsky et al. [38]. However, this question remains unanswered.

Further, the validity of the inequality Eqn 5 as a legitimate base for developing the phase selection rules for HEAs is discussed. In the strictest sense, a solid solution phase is preferred to an intermetallic phase for a multicomponent alloy if $G_{SS} \ll G_{IM}$, where G_{SS} and G_{IM} denote the Gibbs free energy of the solid solution and

worth noting that there may be overlapping areas or empty spaces between adjacent atoms due to the size misfit, which leads to intrinsic residual strain when all atoms are closely packed in a common lattice. (b) The variation of the excess entropy of mixing S_E with the atomic packing fraction ξ for three two-, three-, and four-component model alloys of equiatomic composition. (c) The contour plots of the total configurational entropy of mixing S_T (k_B per atom) for the model Mn–Ni–Fe system at different atomic packing fractions of $\xi = 0, 0.52$, and 0.74 , respectively. Note that 'x' represents the composition with the maximum S_T . (d) The variation of the total entropy of mixing S_T with the atomic packing fraction ξ for three five-component alloys of equiatomic composition.

**FIGURE 5**

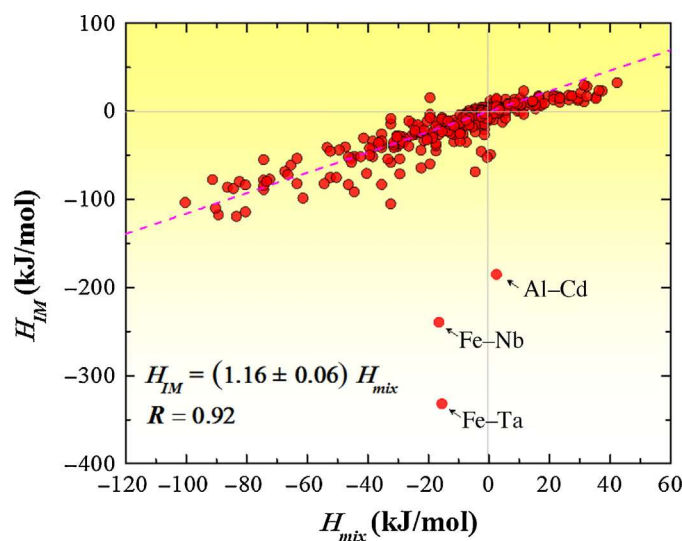
The plot of (a) the Ω values versus phases and (b) the ϕ values versus phases for the HEAs. (c) The plot of the VEC versus ϕ for different HEAs. The FCC solid solution mainly forms around a VEC of 8.5, BCC around a VEC of 5, and HCP around a VEC of 2.8, each within a narrow band.

intermetallic phase, respectively. In terms of entropy and enthalpy, this inequality can be written as $H_{mix} - TS_{mix} \ll H_{IM} - TS_{IM}$, where H and S denote the enthalpy and entropy, respectively, and the subscript IM denotes intermetallics. As $S_{IM} \sim 0$ according to Ref [14], this inequality can be simplified to $TS_{mix} \gg H_{SS} - H_{IM}$. According to previous studies [5,37], H_{mix} is usually approximated using the Miedema formula (Eqn 3). Similarly, if the H_{IM} of a multicomponent alloy can be approximated from the formation enthalpy of the individual binaries [38], we may further simplify the criterion $TS_{mix} \gg H_{SS} - H_{IM}$. In their recent study, Troparevsky et al. [38] obtained the formation enthalpy values for 335 binary intermetallic compounds using the first-principles calculations (the 26 elements considered in their work include Mg, Al, Sc, Ti, V, Cr, Mn, Fe, Co, Ni, Cu, Zn, Y, Zr, Nb, Mo, Rh, Pd, Ag, Cd, La, Hf, Ta, W, Pt, and Au). Similarly, we can plot the obtained H_{IM} and H_{mix} values for the 335 binaries on the same graph. As shown in Fig. 6, it is interesting to note that the values of H_{IM} are positively

correlated ($H_{IM} \sim 1.16H_{mix}$) with the H_{mix} values for most of the binaries studied, except for the three binaries of Al–Cd, Fe–Nb, and Fe–Ta. We obtain the following equation by substituting $H_{IM} \sim 1.16H_{mix}$ into the inequality $TS_{mix} \gg H_{SS} - H_{IM}$:

$$TS_{mix} \gg -0.16H_{mix} \quad (8)$$

On comparing Eqn 8 with Eqn 5, these two criteria are found to be equivalent when $S_{sys} = S_{mix}$ and $\max\{|H_i|\} = -0.16H_{mix}$ are assumed. Note that it is a trivial case for Eqn 8 to hold if H_{mix} is positive. A similar proposal was also made in Ref [38]. However, when extended to ternary, quaternary, and multicomponent alloys, the condition for the formation of ordered compounds could become considerably more complex than simply averaging the formation enthalpy of the binaries. However, a robust and general theoretical model to predict the formation enthalpy of an ordered compound in a multicomponent alloy is currently lacking.

**FIGURE 6**

The formation enthalpy of the binary intermetallic compounds H_{IM} obtained through the first-principles calculations was well correlated with H_{mix} for ~325 atomic pairs formed among 26 metallic elements (Mg, Al, Sc, Ti, V, Cr, Mn, Fe, Co, Ni, Cu, Zn, Y, Zr, Nb, Mo, Rh, Pd, Ag, Cd, La, Hf, Ta, W, Pt, and Au). Only the data for three atomic pairs (Al–Cd, Fe–Nb, and Fe–Ta) are noted to be out of the linear trend.

Valence electron concentration rule

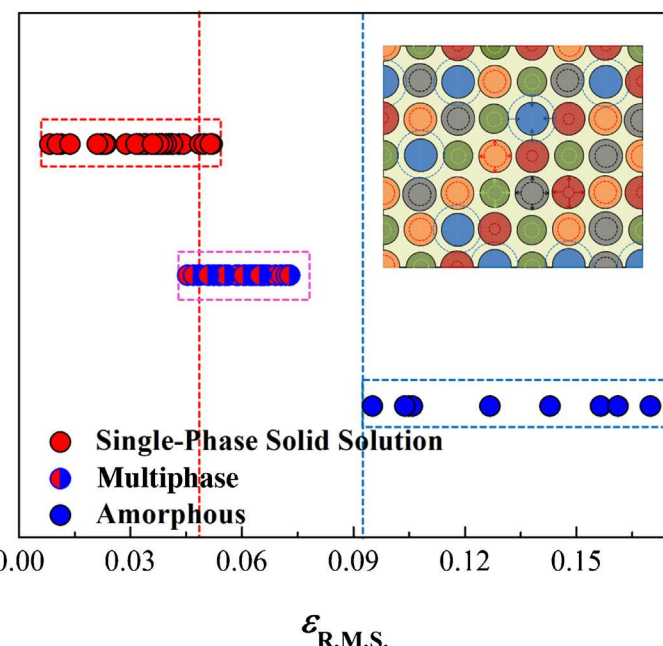
The aforementioned thermodynamic rules prove useful guidelines in selecting phases in HEAs, that is, whether they form a single phase or multiple phases. However, an additional rule or parameter is required for the type of phase, such as FCC, BCC, or hexagonal close packed (HCP), that is formed in an HEA. According to the Hume–Rothery rule [39], the valence electron concentration (VEC) of an alloy constitutes another critical parameter that can influence the crystallinity of a solid solution phase in the absence of a strong atomic size effect [28]. When the d -electrons in the valence band are included, the average VEC of an alloy can be computed as $VEC = \sum_{i=1}^n c_i(VEC)_i$ where $(VEC)_i$ is the VEC for the i th element [28]. Guo et al. [28] and Poletti and Battezzati [40] showed that HEAs with FCC possess a $VEC > 8.0$, whereas those with BCC possess a $VEC > 6.87$. For a holistic analysis, Fig. 5c shows the plot of VEC versus ϕ for a total of ~90 cast HEAs, including a multiphased structure, metallic glasses, as well as single-phase FCC, BCC, and HCP solid solutions that have been discovered recently. Evidently, the VEC of the alloys plays a crucial role in determining the crystallinity of the solid solution phases, particularly for single-phase solid solutions. Within the region of the single-phase solid solution ($\phi > \phi_c \sim 20$), FCC prevails around a VEC of $8.5 \pm (1.0)$, BCC around a VEC of $5 \pm (0.7)$, and HCP around a VEC of $2.8 \pm (0.2)$. However, this clear distinction between phases disappears when the HEAs fall under other phase regions ($\phi < \phi_c$), where other effects such as atomic size difference override the effect of VEC (Fig. 5c).

Intrinsic residual strain and lattice instability

As mentioned previously, in general, mixing different-sized atoms into a common lattice leads to the development of intrinsic residual strains. This is termed as the ‘atomic size rule’ in conventional alloys, a well-known Hume–Rothery rule frequently used to

explain the solubility of solute atoms in an alloy [39]. To rationalize this atomic size effect, Eshelby [41] developed a quantitative micromechanical model a few decades ago based on the continuum elasticity theory, which simply considers solute atoms to solvent atoms as an analogue of inclusions to an elastic medium. However, Eshelby’s approach poses a challenge when applied directly in the study of HEAs, because of their lack of apparent distinction between solvent and solute atoms. To circumvent this problem, a geometric model was recently developed for HEAs [18]. Basically, to prevent the formation of empty spaces or overlapping of atoms in a lattice, as illustrated in Fig. 4a, the size of atoms must be adjusted for dense atomic packing, as manifested by the sharp diffraction peaks obtained from most HEAs. This change in the atomic size gives rise to the intrinsic residual strains, as illustrated by the inset of Fig. 7, which can be deduced by minimizing the atomic packing misfit [18].

Being ‘intrinsic’, these residual strains arise from phase formation and possess a zero average. Therefore, they cannot be detected in a typical XRD spectrum like the residual strains around crystalline defects, the latter of which generally reduces with thermal annealing [42]. However, the fluctuation in these residual strains, as manifested by their root mean square ε_{RMS} , is not zero, which can be correlated with the elastic energy storage in an HEA, serving as the ‘driving force’ for phase transition. As shown in Fig. 7, a cast HEA tends to form a single-phase solid solution if ε_{RMS} is $<5\%$, an amorphous structure if ε_{RMS} is $>10\%$, and a multiphase structure if ε_{RMS} lies between 5% and 10%. These findings are consistent with Lindemann’s criterion of lattice instability [43]. Nevertheless, it should be emphasized that, at best, the criteria based on residual strains are necessary conditions as the chemical effects are neglected.

**FIGURE 7**

The groupings of different-phased HEAs based on their intrinsic root-mean-square (RMS) residual strains. The inset illustrates the atomic size alteration to accommodate close atomic packing atoms in the lattice of a multicomponent alloy, and the dashed cycles indicate the original atomic size, and the arrows indicate the accommodation directions.

Phase selection in HEAs: the computational approach

As mentioned previously, because of the large number of possible HEAs, it would be impossible to look for useful alloys by a trial-and-error method by examining every alloy composition [5,44,45]. Furthermore, the more elements in an alloy the more difficult the construction of its phase diagram. In such cases, in addition to theoretical modeling [4,18,19,27,28], computational approaches, such as density functional theory (DFT) calculations [46] and *ab initio* molecular dynamics (AIMD) [26] simulations, can be used to study phase formation in HEAs. However, due to the significant cost and computational time required for the current technology, among other limitations [5], these approaches are not suitable for high-throughput large-scale screening of alloy compositions in the design of HEAs. Alternatively, a semiempirical computational approach, generally termed as calculations of phase diagrams (CALPHAD), can be used to predict equilibrium phases in HEAs [14,26,30,45]. Based on the existing data obtained from binary and ternary systems, CALPHAD can predict the equilibrium phase(s) of

a multicomponent system by directly computing the minimum Gibbs free energy at a given temperature and pressure [45].

In the CALPHAD formulation, the Gibbs energy of a certain phase ψ is expressed as follows [29]:

$$G^\psi = G_{ref}^\psi + G_{id}^\psi + G_{ex}^\psi \quad (9)$$

where G_{ref}^ψ is the free energy contribution from the pure constituent elements, G_{id}^ψ from the ideal mixing, and G_{ex}^ψ from the excess Gibbs energy of mixing. In theory, G_{id}^ψ is given by the equation $G_{id}^\psi = RT\sum_i c_i \ln c_i$, whereas the excess Gibbs energy term G_{ex}^ψ is written as $G_{ex}^\psi = \sum_i \sum_{j>i} c_i c_j \sum_v v L_{ij}^\psi (c_i - c_j)^v$, where $v L_{ij}^\psi$ is the model parameter that must be determined with the Muggianu geometrical extrapolation scheme [47] using the available experimental data from binary alloys; therefore, this calculation is database dependent. It should be noted that the equation for the excess free energy only holds for binary alloys, possibly varying for ternary, quaternary, and high-order alloys. By minimizing the total Gibbs free energy given in Eqn 9, the stable phase(s) at

TABLE 2

Comparison of phases reported in present as-cast equiatomic high-entropy alloys and calculated results by CALPHAD and φ parameter, respectively.

Experimental results			CALPHAD calculations	φ parameter	
Alloy	Phases reported	Refs	Phases at T_m	φ	Phases predicted
AlCoCrCuFeNi	BCC + FCC	[2]	FCC + B2 + FCC [14]	14.13	Multi
AlCoCrCuNi	BCC + FCC	[33]	B2 + FCC + FCC + BCC [14]	10.06	Multi
AlCoCrCuNi	BCC + FCC + (B2)	[97]	B2 + FCC + FCC + BCC [14]	10.06	Multi
AlCoCrCuNiTi	BCC + Cu + Cr?	[98]	BCC + B2 + B2 + FCC + Ni ₃ Ti [14]	3.41	Multi
AlCoCrFeNi	BCC + B2	[99,100]	B2 + BCC + FCC [14]	5.99	Multi
AlCoCrFeNi	B2 + L1 ₂	[101]	B2 + BCC + FCC [14]	5.99	Multi
AlCoCrFeNiTi	BCC + B2	[100]	BCC + B2 + B2 + FCC + C14 [14]	1.55	Multi
AlCoCuNi	BCC + FCC	[33]	B2 + FCC [14]	5.86	Multi
AlCrCuFeMnNi	BCC	[90]	BCC + B2 + FCC + FCC [14]	13.54	Multi
AlCrCuFeNi	FCC + FCC	[48]	BCC + B2 + FCC [14]	11.40	Multi
AlCrCuFeNiTi	BCC + FCC	[102]	BCC + FCC + C14 + B2 + C15 + NiTi [14]	4.59	Multi
AlCrMnNbTi	Laves + unknown	[14]	BCC [14]	5.59	Multi
AlCrMnNbV	Laves + unknown	[14]	BCC [14]	9.30	Multi
AlCrMoSiTi	B2 + Mo ₅ Si ₃	[27]	Mo ₅ Si ₃ + BCC [14]	-2.07	Intermetallic/amorphous ^a
AlCrMoSiTi	Amorphous	[21]	Mo ₅ Si ₃ + BCC [14]	-2.07	Intermetallic/amorphous ^a
AlCrTiVZr	Compounds	[14]	BCC + B2 [14]	1.16	Multi
AlMnNbTiV	B2 + laves	[14]	BCC [14]	11.26	Multi
AlTiVYZr	Compounds	[9]	AlY ₂ + Al ₂ Zr ₃ + BCC + HCP [14]	1.47	Multi
CoCrCuFeMnNi	FCC	[3]	FCC + FCC [14]	52.56	Single
CoCrCuFeNi	FCC	[2,48]	FCC + FCC [14]	369.34	Single
CoCrCuFeNiTi	FCC + Laves	[70]	BCC + FCC + C14 + Ni ₃ Ti [14]	8.92	Multi
CoCrFeMnNi	FCC	[3]	FCC [14]	34.68	Single
CoCrFeNi	FCC	[103]	FCC [14]	3583.31	Single
CoCuFeNiV	FCC	[9]	FCC + FCC [14]	60.19	Single
CrCuFeMoNi	FCC	[48]	BCC + FCC + BCC [14]	28.97	Single
CrMnNbTiV	Laves + unknown	[14]	BCC + C14 [14]	12.31	Multi
NbMoTaW	BCC	[58]	BCC [14]	60.98	Single
VNbMoTaW	BCC	[58]	BCC [14]	41.17	Single

^a According to Refs, the negative value of φ indicates the tendency of forming intermetallic/amorphous structure.

equilibrium can be finally obtained for a given temperature and pressure. Table 2 lists the experimentally detected phases in the as-cast HEAs compared with the CALPHAD predictions [14] at $T = T_m$ and the theoretical prediction using φ [4]. As seen in Table 2, the experimental results are in general agreement with the φ -parameter predictions. However, a significant discrepancy is noted between the experimental results and the CALPHAD predictions. As explained by Miracle et al. [45], this discrepancy arises from the limitation of the databases used in the CALPHAD computation, or it could suggest that the as-cast phases may not be equilibrium phases.

Before further discussion, the CALPHAD predictions of the HEAs of a single-phase solid solution deserve mention. As discussed in the literature [4,18,19,45], a single-phase solid solution corresponds to a real ‘high-entropy’ effect in HEAs; therefore, it is imperative that materials scientists design a method of obtaining the single-phase solid solution HEAs. As evident from Table 2, the predictions from both the CALPHAD calculation and the φ parameter are in general agreement with the experimental results of single-phase solid solutions. However, a few exceptional cases were noted from among the Fe–Cu-containing alloys, such as CoCrCuFeMnNi [3], CoCrCuFeNi [2,48], CoCuFeNiV [9], and CrCuFeMoNi [48]. As Fe and Cu physically hold a positive enthalpy of mixing, in combination, they are likely to cause elemental segregation inducing local precipitations. For example, minor alloying of Cu in steels was found to result in a large number of homogeneously dispersed nanoprecipitates in the Fe matrix [49]. Similar results were also reported in the Al_{1.3}CoCr-CuFeNi model alloy for the presence of two types of Cu-rich nanoprecipitates through scanning electron microscopy (SEM)-electron backscatter diffraction (EBSD) and energy-dispersive spectroscopy (EDS) analyses; however, these could not be detected even through neutron diffraction analyses [31]. Here, it is worth noting that nanoprecipitation may not contradict the high-entropy effect. Theoretically, entropy is a concept applicable to macroscopic ensembles; therefore, it is not surprising that its effect diminishes at the nanometer scale, with enthalpy rather than entropy playing a more important role.

Properties and prospects

Conventionally, HEAs are defined as alloys comprising more than five principal elements mixed in an equiatomic or near-equiatomic fraction [2,3]. Although the fundamental issues have not yet been completely resolved, such as the thermodynamic origin of phase selection, the designed HEAs were reported to have superior mechanical and physical properties, including ultrahigh fracture

toughness exceeding that of most pure metals and alloys [6], excellent comparable strength to that of structural ceramics and some metallic glasses [50], superconductivity [51], and significant resistance to corrosion [52]. For a general and holistic understanding, Yeh [32] attributed these promising properties to primarily four core effects: (1) the high-entropy effects, which offer the thermodynamics for stabilizing single-phase solid solutions; (2) the sluggish diffusion effect, which retards the growth of second-phase nuclei out of a single-phase solid solution, therefore facilitating the formation of nanoprecipitates; (3) the severe lattice distortion effect, which provides excess strength and also contributes to the slow kinetics in HEAs [5,32]; and (4) the cocktail effect, which could enhance the properties by alloying. These descriptions not only explain the complex phenomena that remain to be elucidated but also provide the useful guidelines for exploring the structure–property correlation in HEAs.

High hardness and superb specific strength

In alloy engineering, the ideal alloy possesses great strength/hardness with a low density [53]. This is of particular interest for structural applications such as in aerospace engineering and civil transports, where controlling the weight of engineering components is critical for reducing the energy demand. In this respect, several research groups have already reported promising results in the development of low-density and high-strength HEAs [50,54,55]. According to Senkov et al. [54], high-hardness and low-density refractory HEAs can be obtained by mixing low-density refractory elements, such as V (6.11 g cm⁻³), Zr (6.51 g cm⁻³), Cr (7.14 g cm⁻³), Nb (8.57 g cm⁻³), and Ti (4.51 g cm⁻³), to form a Cr–Nb–Ti–V–Zr system. These include a series of refractory HEAs with the compositions of NbTiVZr, NbTiV₂Zr, CrNbTiZr and CrNbTiVZr, displaying a very high Vickers microhardness of 3.29, 2.99, 4.10, and 4.72 GPa at a density of 6.52, 6.34, 6.67, and 6.57 g cm⁻³, respectively. According to Senkov et al. [54], these high hardness figures can be attributed to the presence of disordered BCC solid solutions in these refractory HEAs. Furthermore, using a lighter element such as Al to substitute Zr, Stepanov et al. [55] produced an AlNbTiV alloy with a considerably lower density of 5.59 g cm⁻³ and a coarse-grained single-phase BCC structure. As a result, the compressive yield strength of this alloy is significantly high, reaching up to 1.02 GPa at an ambient temperature. More recently, Youssef’s group [50] developed a novel nanocrystalline Al₂₀Li₂₀Mg₁₀Sc₂₀Ti₃₀ HEA with an HCP structure via mechanical alloying, with a super-low density

TABLE 3

Properties of novel solid-solution HEAs such as Al₂₀Li₂₀Mg₁₀Sc₂₀Ti₃₀ [50], low-density refractory HEAs (Cr–Nb–Ti–V–Zr system) [54], and CrMnFeCoNi (77 K) [6] compared with other metallic alloys [53,73].

Properties	Al ₂₀ Li ₂₀ Mg ₁₀ Sc ₂₀ Ti ₃₀	Low-density refractory HEAs	CrMnFeCoNi (77 K)	Vit1	Al alloys	Ti alloys	Steel alloys
Density (g cm ⁻³)	2.67	6.34–6.67		6.1	2.6–2.9	4.3–5.1	7.8
Hardness (GPa)	5.9	2.99–4.72		5.7	0.20–1.75	0.54–3.80	1.50–4.80
Yield strength, σ_y (GPa)	1.97^a	1.00–1.57	0.73	1.9	0.10–0.63	0.18–1.32	0.50–1.60
Specific strength (GPa g ⁻¹ cm ³)	0.74	0.16–0.24		0.32	<0.24	<0.31	<0.21
Fracture toughness (MPa m ^{1/2})			200–300	20–140	23–45	55–115	50–154

The bold values represent the best properties of the materials listed in Table.

^aThe yield strength is estimated by dividing hardness by three.

($<3 \text{ g cm}^{-3}$) but ultra-high strength ($\sim 2 \text{ GPa}$), as estimated by dividing the hardness value by three. As seen in Table 3, this low-density $\text{Al}_{20}\text{Li}_{20}\text{Mg}_{10}\text{Sc}_{20}\text{Ti}_{30}$ HEA is about two to three times stronger than nanocrystalline Al alloys and even stronger than the metallic glass Vit1. Furthermore, because of its ultralow density ($\sim 2.67 \text{ g cm}^{-3}$), the $\text{Al}_{20}\text{Li}_{20}\text{Mg}_{10}\text{Sc}_{20}\text{Ti}_{30}$ HEA exhibits excellent specific strength of $\sim 0.74 \text{ GPa g cm}^{-3}$, which is comparable to that of SiC ceramics [50] and several times higher than those of conventional light alloys, such as Al alloys and Ti alloys (Table 3).

Superior mechanical performance at elevated temperatures

As discussed earlier, the high mixing entropy in HEAs at elevated temperatures promotes the formation of single-phase solid solutions [5,15,51,56,57]. Therefore, this is conducive to the development of high-temperature structural alloys [5,15,56,57], which can achieve excellent mechanical performance at high temperatures due to the sluggish diffusion of their constituent elements [5,57]. Figure 8 shows the yield strengths of the single-phase refractory HEAs [58,59] (with a BCC structure) compared with those of two conventional superalloys, namely Inconel 718 and Haynes 230, designed for applications at high temperature [58]. From this figure, it is evident that the Inconel 718 superalloy has a strength comparable to the refractory HEAs at low temperatures. However, it significantly thermo-softens once the temperature rises above 600°C ; in sharp contrast, the refractory HEAs are able to display high strength ($>1 \text{ GPa}$) even at a temperature of 1200°C . Furthermore, recent works [54,56] have shown that, in addition to good performance at high temperatures, the density of the refractory HEAs can be significantly reduced by replacing heavy elements, such as Ta and W, with light elements, such as Cr, Ti and Al. According to Ref [54], the density of the new refractory CrNbTiVZr HEA could be as low as 6.57 g cm^{-3} , which is comparable to that of Ti alloys and thus critical for applications in aerospace engineering. By completely substituting Cr with Al in $\text{CrMo}_{0.5}\text{NbTa}_{0.5}\text{TiZr}$, the density can be considerably reduced by 10.1%, while maintaining a yielding strength up to 2000 MPa at 298 K and 745 MPa at 1273 K, resulting in a very high specific yield strength both at room temperature and at high temperatures [56,60].

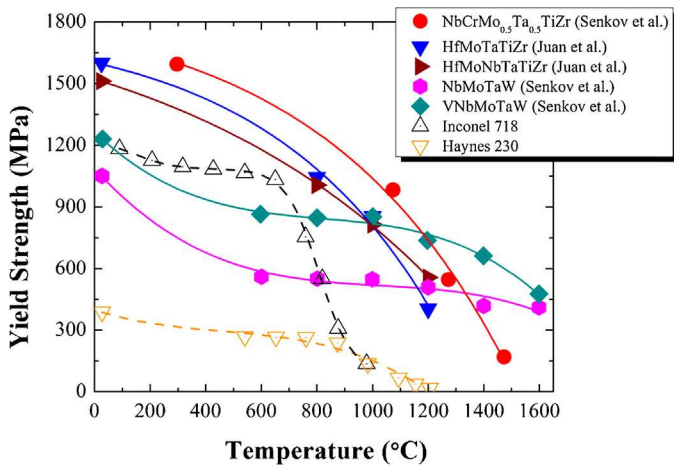


FIGURE 8

The temperature dependence of the yield strength of $\text{NbCrMo}_{0.5}\text{Ta}_{0.5}\text{TiZr}$ [58], HfMoTaTiZr [59], HfMoNbTaTiZr [59], NbMoTaW [58], and VNbMoTaW [58] refractory HEAs compared with those of two typical superalloys, Inconel 718 and Haynes 230 [58].

Exceptional ductility and fracture toughness at cryogenic temperatures

It has long been considered that increasing the strength of conventional alloys will result in the loss of ductility and vice versa, which is known as the ‘strength–ductility paradox’ and has been observed in many types of alloys [53,61], as shown in Fig. 9. Therefore, materials scientists have endeavored to develop alloys with both high strength and high ductility, for example, by grain refinement with nanotwins [61–63] and the development of gradient microstructures [61,63,64]. The stacking fault energy (SFE) of metals/alloys is significant in the promotion of twinning. In general, the lower the SFE the easier the generation of twining [6,65–67]. Interestingly, the SFE in some HEAs was found to be extremely small ($\sim 3.5 \text{ mJ/m}^2$) [66], even lower than those in 304L steel [66] ($\sim 18 \text{ mJ/m}^2$) and Cu–Al–Zn alloys [66] ($\sim 7 \text{ mJ/m}^2$). Physically, a low SFE facilitates the splitting of full dislocations into partials [66], thus suppressing dislocation cross-slip and climb. Consequently, a high yield strength can be attained for alloys with a low SFE [6,65–68]. Low SFE can also lead to twinning-mediated plasticity [66–68], hence resulting in high ductility under appropriate conditions [62,66–68].

Recently, Gludovatz et al. [6] investigated a CrMnFeCoNi HEA with a single-phase FCC structure and an SFE of 25 mJ/m^2 . Interestingly, although no nanotwinning was noted when the HEA was plastically deformed at the ambient temperature, the plasticity mechanism was found to shift from dislocation planar slip to nanotwinning with decreasing temperature. As a result, this HEA displays excellent tolerance to damage with a high tensile strength ($>1 \text{ GPa}$) and superior fracture toughness ($>200 \text{ MPa m}^{1/2}$) even at a cryogenic temperature of 77 K , which is considerably superior to most metallic alloys [6], as listed in Table 3. Conversely, Deng et al. successfully synthesized a four-component $\text{Fe}_{40}\text{Mn}_{40}\text{Co}_{10}\text{Cr}_{10}$ alloy that undergoes mechanically induced twinning upon plastic deformation even at room temperature. This alloy

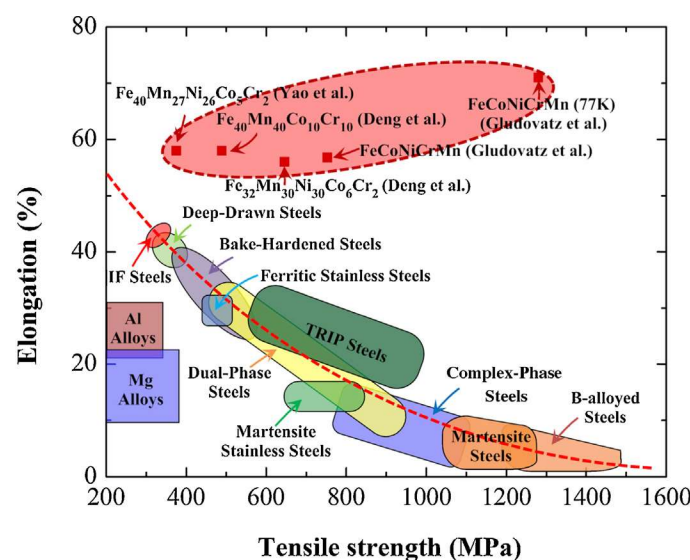


FIGURE 9

Strength versus ductility properties for low-SFE HEAs such as $\text{Fe}_{40}\text{Mn}_{27}\text{Ni}_{26}\text{Co}_5\text{Cr}_2$ [74], $\text{Fe}_{40}\text{Mn}_{40}\text{Co}_{10}\text{Cr}_{10}$ [65], $\text{Fe}_{32}\text{Mn}_{30}\text{Ni}_{30}\text{Co}_6\text{Cr}_2$ [65], and FeCoNiCrMn [6] at room temperature and FeCoNiCrMn [6] at 77 K , compared with other conventional alloys [75].

possesses a single-phase FCC solid solution structure with comparable tensile properties to that of the CrMnFeCoNi HEA [65]. As seen in Fig. 9, the single-phase low-SFE HEAs clearly exhibit a trend of ‘the stronger being more ductile’, which is contrary to the behaviors of most conventional alloys known to date. Here, it is worth noting that nanotwinning may not be the only strengthening mechanism responsible for this unusual mechanical behavior; solid solution strengthening has also been found to play an important role.

Novel functional properties

In addition to their promising mechanical properties, some HEAs also exhibit interesting functional properties due to their high configurational entropy, which limits precipitation, if any, at a nanometer scale [69]. For instance, both $Ti_{0.8}CoCrCuFeNi$ and $TiCoCrCuFeNi$ HEAs were reported to have superparamagnetic properties [70], and the $Ta_{34}Nb_{33}Hf_8Zr_{14}Ti_{11}$ HEA [51] with an average BCC structure was also found to display superconductivity at the critical temperature of $T_c \approx 7.3$ K. This suggests that the HEA could be used in strong superconducting electromagnets such as magnetic resonance imaging (MRI) scanners, nuclear magnetic resonance (NMR) machines, and particle accelerators, like several other type II superconductors. Although the physical mechanisms underlying these interesting phenomena remain to be elucidated [51], the combination of promising physical properties, such as high saturation magnetization, electrical resistivity, and malleability, as well as low coercivity, points to the great potential of HEAs as functional materials.

Summary and outlook

The advent of HEAs, which are composed of multiple principal elements unlike conventional alloys with one and rarely two base elements, point to a paradigmatic shift in the design of modern alloys. The mechanical/physical/chemical properties of HEAs, as novel alloys, are yet to be investigated. However, challenges related to the fundamental issues have emerged, such as the formation of different phases in HEAs. In addition, due to the exceedingly high number of possible compositions for HEAs, although only a few may prove useful, identifying useful alloy compositions via the traditional trial-and-error method has become difficult, which calls for an efficient high-throughput method for alloy screening [4,14,38]. In turn, this has led to the recent development of new theories, models, and methods that apply not only to conventional alloys but also to HEAs [4,18,28,38,40,71]. Despite these recent advancements, the atomistic mechanisms governing phase formation in HEAs must be investigated further.

In spite of these challenges, the HEAs were found to have novel properties such as superb specific strength, excellent mechanical performance at high temperature, exceptional ductility and fracture toughness at cryogenic temperatures, superparamagnetism, and superconductivity. These properties are promising for new discoveries and inventions in future, which may ultimately lead to new applications. For instance, HEAs as light as Al alloys but stronger than some metallic glasses [50] can be used in the transportation industry and energy sectors, where lightweight high-strength materials are in great demand [45]. HEAs containing refractory elements such as Nb, Mo, and Ta can maintain their high strength even above 1200°C, superior to traditional superalloys such as Inconel 718 and

Haynes 230 [58]. These HEAs can be used in high-temperature applications, such as gas turbines, rocket nozzles, and nuclear construction [72]. Low-density refractory HEAs can also be applied in the aerospace industry, where lightweight materials tolerant to high temperatures are in demand [58]. The outstanding cryogenic properties of HEAs make them an excellent choice for cryogenic applications such as rocket casings, pipework, and liquid O₂ or N₂ equipment [72]. In view of these promising findings, we believe that more HEAs with promising properties can be discovered with further advancements, thereby promoting the applications of metallic material in industries, which were previously limited.

Acknowledgments

YY is grateful for the financial support provided by the Hong Kong Government through the General Research Fund (GRF) with the grant number of CityU11207215 and through the joint GRF-NSFC fund with the grant number of N_CityU116/14.

References

- [1] R.E. Hummel, Understanding Materials Science, second ed., Springer-Verlag, 2004.
- [2] J.W. Yeh, et al. *Adv. Eng. Mater.* 6 (5) (2004) 299.
- [3] B. Cantor, et al. *Mater. Sci. Eng. A* 375–377 (2004) 213.
- [4] Y.F. Ye, et al. *Scripta Mater.* 104 (2015) 53.
- [5] Y. Zhang, et al. *Progr. Mater. Sci.* 61 (2014) 1.
- [6] B. Gludovatz, et al. *Science* 345 (6201) (2014) 1153.
- [7] M.A. Hemphill, et al. *Acta Mater.* 60 (16) (2012) 5723.
- [8] S.Q. Xia, et al. *JOM* (2015) 1.
- [9] Y. Zhang, et al. *Adv. Eng. Mater.* 10 (6) (2008) 534.
- [10] R.A. Swalin, Thermodynamics of Solids, Wiley, 1962.
- [11] K. Guan-Yu, et al., FCC and BCC equivalents in as-cast solid solutions of $Al[x]Co[y]Cr[z]Cu[0.5]Fe[v]Ni[w]$ high-entropy alloys, Cachan, France, 2006. p. 669.
- [12] H.Y. Ding, K.F. Yao, *J. Non-Crystal. Solids* 364 (1) (2013) 9.
- [13] J.Y. He, et al. *Acta Mater.* 62 (2014) 105.
- [14] O.N. Senkov, et al. *Nat Commun.* (2015) 6.
- [15] O.N. Senkov, et al. *Intermetallics* 18 (9) (2010) 1758.
- [16] A. Takeuchi, et al. *JOM* 66 (10) (2014) 1984.
- [17] R.A. Oriani, Advances in Chemical Physics, John Wiley & Sons, Inc., 2007. p. 119.
- [18] Y.F. Ye, et al. *Intermetallics* 59 (2015) 75.
- [19] A. Takeuchi, et al. *Entropy* 15 (2013) 3810.
- [20] A. Inoue, et al. *J. Non-Crystal. Solids* 156–158 (Pt 2) (1993) 473.
- [21] S. Guo, C.T. Liu, *Progr. Nat. Sci.: Mater. Int.* 21 (6) (2011) 433.
- [22] G.A. Mansoori, et al. *J. Chem. Phys.* 54 (4) (1971) 1523.
- [23] A. Luca, F. Giuseppe, *J. Phys.: Condens. Matter* 19 (25) (2007) 256207.
- [24] S. Singh, et al. *Acta Mater.* 59 (2011) 182.
- [25] A. Takeuchi, et al. *Intermetallics* 19 (10) (2011) 1546.
- [26] M. Gao, D. Alman, *Entropy* 15 (10) (2013) 4504.
- [27] X. Yang, Y. Zhang, *Mater. Chem. Phys.* 132 (2/3) (2012) 233.
- [28] S. Guo, et al. *J. Appl. Phys.* 109 (10) (2011).
- [29] H. Lukas, Suzana G. Fries, B. Sundman, Computational Thermodynamics, Cambridge University Press, 2007.
- [30] C. Zhang, et al. *JOM* 64 (7) (2012) 839.
- [31] L.J. Santodonato, et al. *Nat Commun.* (2015) 6.
- [32] J.W. Yeh, *Eur. J. Control* 31 (6) (2006) 633.
- [33] J.W. Yeh, et al. *Mater. Chem. Phys.* 103 (1) (2007) 41.
- [34] J.W. Yeh, et al. *Metall. Mater. Trans. A: Phys. Metall. Mater. Sci.* 35 (8) (2004) 2533.
- [35] C.J. Tong, et al. *Metall. Mater. Trans. A: Phys. Metall. Mater. Sci.* 36 (4) (2005) 881.
- [36] L. Liu, et al. *Mater. Des.* 44 (2013) 223.
- [37] Y. Zhang, et al. *MRS Commun.* 4 (2) (2014) 57.
- [38] M.C. Troparevsky, et al. *Phys. Rev. X* 5 (1) (2015) 011041.
- [39] U. Mizutani, Hume-Rothery Rules for Structurally Complex Alloy Phases, CRC Press, 2010.
- [40] M.G. Poletti, L. Battezzati, *Acta Mater.* 75 (2014) 297.

- [41] J.D. Eshelby, in: S. Frederick, T. David (Eds.), *Solid State Physics*, vol. 3, Academic Press, 1956, p. 79.
- [42] W.F. Smith, J. Hashemi, *Foundations of Materials Science and Engineering*, McGraw-Hill, 2003.
- [43] F.A. Lindemann, *Physik. Z.* 11 (1910) 609.
- [44] B. Cantor, *Entropy* 16 (9) (2014) 4749.
- [45] D. Miracle, et al., *Entropy* 16 (1) (2014) 494.
- [46] W. Kohn, L.J. Sham, *Phys. Rev.* 140 (4A) (1965) A1133.
- [47] Y.M. Muggianu, et al., *J. Chim. Phys.* 72 (1975) 83.
- [48] C. Li, et al., *J. Alloys Compd.* 475 (1/2) (2009) 752.
- [49] Y.R. Wen, et al., *Acta Mater.* 61 (20) (2013) 7726.
- [50] K.M. Youssef, et al., *Mater. Res. Lett.* 3 (2) (2014) 95.
- [51] P. Koželj, et al., *Phys. Rev. Lett.* 113 (10) (2014) 107001.
- [52] C.P. Lee, et al., *J. Electrochem. Soc.* 154 (8) (2007) C424.
- [53] M.F. Ashby, in: M.F. Ashby (Ed.), *Materials Selection in Mechanical Design*, fourth ed., Butterworth-Heinemann, 2011, p. 97.
- [54] O.N. Senkov, et al., *Acta Mater.* 61 (5) (2013) 1545.
- [55] N.D. Stepanov, et al., *Mater. Lett.* 142 (2015) 153.
- [56] O.N. Senkov, et al., *Acta Mater.* 68 (2014) 214.
- [57] K.Y. Tsai, et al., *Acta Mater.* 61 (13) (2013) 4887.
- [58] O.N. Senkov, et al., *Intermetallics* 19 (5) (2011) 698.
- [59] C.-C. Juan, et al., *Intermetallics* 62 (2015) 76.
- [60] O.N. Senkov, et al., *JOM* 66 (10) (2014) 2030.
- [61] K. Lu, *Science* 345 (6203) (2014) 1455.
- [62] K. Lu, et al., *Science* 324 (5925) (2009) 349.
- [63] H. Kou, et al., *Adv. Mater.* 26 (31) (2014) 5518.
- [64] X. Wu, et al., *Proc. Natl. Acad. Sci. U. S. A.* 111 (20) (2014) 7197.
- [65] Y. Deng, et al., *Acta Mater.* 94 (2015) 124.
- [66] A.J. Zaddach, et al., *JOM* 65 (12) (2013) 1780.
- [67] P.-L. Sun, et al., *Mater. Sci. Eng. A* 525 (1/2) (2009) 83.
- [68] Y.L. Gong, et al., *Mater. Sci. Eng. A* 569 (2013) 144.
- [69] X.D. Xu, et al., *Acta Mater.* 84 (2015) 145.
- [70] X.F. Wang, et al., *Intermetallics* 15 (3) (2007) 357.
- [71] Y.F. Ye, et al., *Acta Mater.* 94 (2015) 152.
- [72] M.F. Ashby, et al., *Materials: Engineering, Science, Processing and Design*, Elsevier Science, 2007.
- [73] M. Telford, *Mater. Today* 7 (3) (2004) 36.
- [74] M.J. Yao, et al., *Scripta Mater.* 72–73 (2014) 5.
- [75] S. Rajasekharan, et al. in: Y. Weng, et al. (Eds.), *Advanced Steels*, Springer, 2011, p. 371.
- [76] M.-R. Chen, et al., *Mater. Trans.* 47 (5) (2006) 1395.
- [77] Y.F. Kao, et al., *J. Alloys Compd.* 488 (1) (2009) 57.
- [78] C. Ng, et al., *J. Alloys Compd.* 584 (2014) 530.
- [79] Z. Wu, et al., *Intermetallics* 46 (2014) 131.
- [80] C.C. Tung, et al., *Mater. Lett.* 61 (1) (2007) 1.
- [81] M.-R. Chen, et al., *Metall. Mater. Trans. A* 37 (5) (2006) 1363.
- [82] L. Liu, et al., *Mater. Sci. Eng. A* 548 (2012) 64.
- [83] B. Ren, et al., *J. Alloys Compd.* 493 (1/2) (2010) 148.
- [84] S. Guo, et al., *J. Alloys Compd.* 557 (2013) 77.
- [85] Y.J. Zhou, et al., *Appl. Phys. Lett.* 92 (24) (2008) 241915.
- [86] T.-T. Shun, et al., *J. Alloys Compd.* 493 (1/2) (2010) 105.
- [87] X. Yang, et al., *Procedia Eng.* 36 (2012) 292.
- [88] M. Feuerbacher, et al., *Mater. Res. Lett.* 3 (1) (2014) 1.
- [89] G.Y. Ke, et al., *Ann. Chim. Sci. Mater.* 31 (6) (2006) 669.
- [90] H.-Y. Chen, et al., *Ann. Chim. Sci. Mater.* 31 (6) (2006) 685.
- [91] L. Jiang, et al., *Intermetallics* 44 (2014) 37.
- [92] F.J. Wang, et al., *J. Alloys Compd.* 478 (1/2) (2009) 321.
- [93] Y.X. Zhuang, et al., *Mater. Sci. Eng. A* 572 (2013) 30.
- [94] K.-C. Hsieh, et al., *J. Alloys Compd.* 483 (1/2) (2009) 209.
- [95] X.Q. Gao, et al., *J. Non-Crystal. Solids* 357 (21) (2011) 3557.
- [96] L. Ma, et al., *Mater. Trans.* 43 (2) (2002) 277.
- [97] U.S. Hsu, et al., *Mater. Sci. Eng. A* 460–461 (2007) 403.
- [98] Z. Hu, et al., *Mater. Des.* 31 (3) (2010) 1599.
- [99] Y. Zhang, et al., *Metall. Mater. Trans. A* 43 (8) (2012) 2625.
- [100] Y.J. Zhou, et al., *Appl. Phys. Lett.* 90 (18) (2007) 181904.
- [101] C. Li, et al., *J. Appl. Phys.* 104 (11) (2008) 113504.
- [102] M. Chen, et al., *Acta Metall. Sin.* 43 (2007) 1020.
- [103] Y.-J. Hsu, et al., *Mater. Chem. Phys.* 92 (1) (2005) 112.